SS-31 Modification Inhibits Pro-inflammatory Effect of Macrophages Induced by Superparamagnetic Iron Oxide Nanoparticles

Qizheng Lu
Tongji University School of Medicine
Haibo Liu
Fudan University
Hao Zheng
Tongji University School of Medicine
Youming Zhang
Tongji University School of Medicine
Jinbo Ou
Tongji University School of Medicine
Jieyun You
Tongji University School of Medicine
Qi Zhang
Tongji University School of Medicine
Jingjiang Pi
Tongji University School of Medicine
Xiaobo Yao
Tongji University School of Medicine
Jing Xu
Tongji University School of Medicine
Xingxu Wang
Tongji University School of Medicine
Yunkai Wang
Tongji University School of Medicine
Ning Pei
Shanghai University
Yunli Shen (shenyunli2011@163.com)
Tongji University School of Medicine

Research Article

Keywords: mitochondria-targeted antioxidant peptide, superparamagnetic iron oxide

Posted Date: May 12th, 2022

DOI: https://doi.org/10.21203/rs.3.rs-1624695/v1

Abstract

Superparamagnetic iron oxide nanoparticles (SPION) could induce macrophage polarization into the pro-inflammatory M1-like subtype. The adverse effect is very likely to restrict the diagnostic or therapeutic applications of SPION in the cardiovascular field. To inhibit the pro-inflammatory effect, a mitochondrial targeted antioxidant peptide SS-31 modifying SPION (SPION@SS-31) was constructed. The macrophages (RAW 264.7) were incubated with SPION or SPION@SS-31 at the concentration of 50 μg Fe_3O_4/mL for 24 hours. Compared to the SPION group, the SPION@SS-31 group demonstrated significantly reduced macrophage damage, evidenced by maintained cell viability, a decrease of early cells apoptosis and reactive oxygen species (ROS) production. Moreover, the pro-inflammatory factor TNF-α and M1-like cell surface markers CD86 and CD80 were significantly down-regulated in the SPION@SS-31 group. Notably, higher levels of anti-inflammatory factors IL-10 and TGF-β and M2-like cell surface marker CD163 were detected in the SPION@SS-31 group by enzyme-linked immunosorbent assay (ELISA) and flow cytometric analysis. Besides, severe disruption of mitochondrial microstructure was observed by transmission electron microscope (TEM) in the SPION group, but less in the SPION@SS-31 group. Co-loading mitochondria-targeted antioxidant peptide SS-31 could significantly mitigate the pro-inflammatory effect of macrophages induced by SPION, indicating that the modification strategy has the potential to promote macrophages M2-like polarization in vitro study.

Introduction

Superparamagnetic iron oxide nanoparticles (SPION) have been widely used as magnetic resonance contrast agents [1], cell tracers [2], and magnetic targeted therapy carriers [3, 4] in the diagnostic or therapeutic studies of cardiovascular diseases. The most representative SPION, such as ferumoxytol, have been approved by FDA for clinical applications [5], including vascular and plaque imaging [6], identification of heart transplantation rejection [7] and evaluation of inflammatory response following acute myocardial infarction [8], acute myocarditis [9] and acute stress-induced cardiomyopathy (Takotsubo cardiomyopathy) [10], indicating that SPION have great potential applications in the cardiovascular field. Correspondingly, the cardiovascular safety of SPION has attracted more and more attention [11].

Previous studies have confirmed that SPION can induce macrophages to polarize into pro-inflammatory M1 subtype [12], potentiating macrophage-modulating cancer immunotherapies [13]. It is well known that macrophages are the main inflammatory cells both in the development of atherosclerosis and in the inflammatory reaction after myocardial infarction. The polarity transition of macrophages from M1 to M2 is of great significance for promoting the repair of infarcted myocardium and maintaining the stability of atherosclerotic plaque [14, 15]. Thus, there is a reasonable concern that SPION could prevent the repair of infarcted myocardium or provoke plaque instability for it is likely to impede the polarity transition of macrophages by inducing prolonged pro-inflammatory effect, when applied for diagnosis or treatment of coronary atherosclerotic heart disease. It is now well accepted that oxidative stress is the main mechanism of SPION induced cytotoxicity [16, 17]. Mitochondria are the largest iron metabolism

organelles and the main sites for ROS production in cells [18]. Thus, we speculated that mitochondria might be the primary organelles attacked by SPION after engulfed and degraded into free iron. Mitochondrial targeted antioxidant peptide SS-31 has been proved to be the most effective SS peptide to protect against ischemia-reperfusion injury through scavenging ROS and inhibiting ROS production [19, 20]. Global multicenter clinical trials have also confirmed that SS-31 is safe and well-tolerated in patients with acute ST-segment elevation myocardial infarction [21]. Furthermore, compared with other mitochondrial targeting antioxidants, such as triphenylphosphine Mito Q, the mitochondrial targeting ability of SS-31 is not prone to be affected by membrane potential depolarization [22]. We presume that SS-31 modifying SPION may be a promising strategy to improve the pro-inflammatory effect of SPION. Here, to overcome the macrophage toxicity of SPION, we developed SPION modified by SS-31 (SPION@SS-31) and verified whether SS-31 modification could mitigate the pro-inflammatory effect of SPION in vitro study.

Material And Methods

Preparation of SPION@SS-31

The schematic diagram of the synthesis of SPION@SS-31 was shown in Fig. 1. In brief, SPION was synthesized according to the method in previous studies [23, 24]. The collected SPION was washed, filter sterilized and suspended into 20 mg/ml using sterile water. After that, SS-31 (5 mg) (All peptide, China) and PEI 1600 (10 mg) (Adamas-beta, China) were added into 1ml sterile water and stirred for 1 hour to get the PEI 1600@ SS-31 mixture. Then, the PEI 1600@SS-31 and SPION were mixed, stirred and reacted for 2 hours. The end product SPION@SS-31 was obtained after washing and removing non-loaded SS-31 by centrifugation using ultrafiltration centrifugal tubes (Millipore, USA). Dynamic light scattering (DLS) measurements were performed on a Zeta sizer Nano instrument (Malvern, UK) at 298 K to analyze the hydrodynamic diameters and Zeta potential of SPION@SS-31. Morphology of SPION@SS-31 was detected using a JEM 2010 (JEOL, Japan) TEM instrument with 200 kV accelerated voltage. A vibrating sample magnetometer (VSM, Lake Shore 7400 system, USA) was employed to analyze saturation magnetization and M-H loop measurements under the magnetic field (H) up to 18,000×g. SPION@SS-31 (10 mg) were suspended in the 10kDa dialysis bag and detected the SS-31 concentration at 37℃ at various time points by Bicinchoninic Acid method on a NanoDrop 1000 spectrophotometer (Thermo Scientific, USA). The SS-31 release curves were obtained by calculating the release percentage and plotting the cumulative drug release against time.

[Figure 1 near here]

Cell Culture and treatment

The classical macrophages cell line (RAW 264.7) was acquired from the Stem Cell Bank (Chinese Academy of Sciences, China). The cells were maintained in high glucose Dulbecco's Modified Eagle Medium (D-MEM) (Hyclone, USA) containing 100 U/mL penicillin, 100 μg/mL streptomycin, 4 mmol/L glutamine, and 10% fetal bovine serum (Gibco, USA). The cells were cultured at 37°C in a humidified

atmosphere of 5% CO2. The macrophages were washed in the serum-free medium and then randomly divided into three groups. Except for the control group, which was not treated with any nanoparticles, the other two groups of macrophages were incubated with SPION or SPION@ SS-31 at the concentration of 50 μg/ml (normalized to Fe_3O_4 content) for 24 hours, respectively.

Detection of Macrophage Phagocytosis

Prussian blue staining was performed to confirm SPION to be internalized by macrophages. Briefly, after different treatments, the slides were fixed with 4% paraformaldehyde for 15 min. After three washes with PBS, the slides were stained using the Prussian blue staining solution kit (Servicebio, China) for 1 hour. Then stained sides were washed with running water, followed by dehydration through alcohol, xylene transparent and sealing. Iron staining was observed under the light microscope (Leica DFC500, Germany).

The representative iron phagocytosis of macrophages incubated with SPION@SS-31 was examined by scanning electron microscope (SEM). After fixing for 2 hours at room temperature, cover slides were washed with 0.1M PB (pH 7.4) for 3 times, 15 min each. Then slides were transferred into 1% OsO4 in 0.1 M PB (pH 7.4) for 2 hours at room temperature. After that, cover slides were rewashed and dehydrated with gradient alcohol for 15 min each time. Finally, ethanol was substituted with a graded isoamyl acetate series. Samples were dried with Critical Point Dryer (HITACHI MC1000, Japan). Specimens were attached to metallic stubs using carbon stickers and sputter-coated with gold for 30s, observed and took images with the scanning electron microscope. (HITACHI SU8100, Japan).

Observation of Cell Morphology

The morphology of macrophages incubated with SPION, SPION@SS-31 and culture medium were examined by flow cytometry. Macrophages were harvested after different treatments. Afterward, macrophages were washed twice with PBS, resuspended, counted, and analyzed using a flow cytometer (AriII BD Biosciences, USA). For cell size and structure analysis, flow cytometric forward scatter (FSC) and side scatter (SSC) density plots were applied.

The morphology changing of macrophages was verified again examined by SEM. Macrophages were fixed and prepared for scanning electron microscope as previously described. Pictures of representative different macrophage morphology were also captured with different magnification.

Determination of Cell Viability

Cell viability was performed using Cell Counting Kit-8 (CCK-8) colorimetric assay (APExBIO, USA), according to the manufacturer's instruction. Absorbance was read at 450 nm. Cell viability (%) = OD (treated cells)/OD (control cells) × 100.

Measurement of Mitochondrial Morphology

The mitochondrial morphology was observed by TEM. Macrophages were fixed and embedded. After that, ultrathin sections were cut to 60–80 nm thin on the ultra-microtome (Leica UC7, Germany), fished

out onto the 150 meshes copper grids with formvar film, dehydrated in a series of gradient ethanol and embedded in epoxy resin. The samples were then stained with 2% uranyl acetate and 2.6% lead citrate and observed using a transmission electron microscope (HITACHI HT7800, Japan). The mitochondrial Flameng score was used to assess the mitochondrial structural damage. The score of the 100 mitochondria per layer was calculated in average. Flameng Score: 0–4 points represent mild to severe mitochondrial structural damage ordinately [25].

Evaluation of Mitochondrial ROS

Macrophages were implanted in 6-well plates and incubated with different nanoparticles for 24 hours. MitoSOX (Thermo Fisher, USA) was dissolved in PBS to make a 5 μM working solution. 1 mL of working solution was applied to cover cells adhering to 6-well plates. Cells were incubated for 10 min at 37°C and 5% CO2 in the dark. After being washed gently three times with PBS, macrophages were observed under the fluorescence microscope.

Flow Cytometry

The Annexin V-FITC Apoptosis Detection Kit (BD Biosciences, USA) was employed to detect apoptotic cells. Cell lines were seeded in 6-well plates at about 50% confluence, then adhered and cultured for 12 hours. Macrophages were treated with the different nanoparticles and culture medium for 24 hours. Subsequently, macrophages were washed with PBS and resuspended in Annexin-V binding buffer. Then, macrophages were stained with Annexin-V-FITC and propidium iodide and incubated in the dark before analysis. Samples were evaluated by flow cytometry within 30 min.

Production of reactive oxygen species (ROS) assessment was assessed by flow cytometry in response to various treatments. Briefly, macrophages were collected at 24 hours after different treatments, loaded with 5 μM H2DCFDA (Sigma, USA) in the dark for 30 min at 37°C, washed twice, and evaluated by flow cytometry.

Mitochondrial ROS were detected using MitoSOX (Invitrogen, USA). Macrophages were incubated with 5 μM MitoSOX for 10 min, as previously described. Cells were collected, washed, measured by flow cytometry. The generation of mitochondrial ROS was expressed as the median fluorescence intensity (MFI) of MitoSOX.

Expression of CD80, CD86, CD206 and CD163 on macrophages were analyzed by flow cytometry. Fc receptors were blocked using Fc-Block™ (BD Biosciences, USA) After two washes with cold PBS, cells (1×105) were harvested in PBS, resuspended and stained with anti-CD80 (BD Biosciences, USA), anti-CD86 (Biolegend, USA) surface antibodies. To detect intracellular CD206 and CD163, stained cells were washed 2 times with staining buffer, fixed and permeabilized with Cytofix/Cytoperm kit (BD Biosciences, USA), and then stained with anti-CD206 (BD Biosciences, USA) and anti-CD163 (Biolegend, USA) antibodies for 30 min at 4°C. Samples were washed, resuspended and performed flow cytometric analysis.

At least 10,000 cells were measured per individual sample. The following gating strategy was applied. FSC/SSC gating included all visible cell populations. Subsequently, dead cells and cell debris were excluded. The doublets and clumps being gated out ensued. Fluorescent minus one samples were used for gating strategy controls. After defining gating strategy on control cells all gating was applied uniformly to all samples. All flow cytometry was measured on a BD AriII flow cytometer, and analysis was implemented using FlowJo (version 10).

Enzyme-Linked Immunosorbent Assay

ELISA was employed to detect the concentrations of TNF-α, TGF-β, IL-6 and IL-10 using ELISA kits (Multi Sciences, China) complying with the manufacturer's instructions. Briefly, recombinant standards or diluted cell-free supernatants were added into the pre-coated antibody 96-well microplate and incubated with detection antibody for 1.5 hours. After washing, streptavidin-HRP was added and incubated for 30 min. The substrate was added for 20 min for color development after washing, followed by adding the stop solution to stop the reaction. The optical density (OD) of each well was determined at 450 nm. The concentrations of soluble cytokines in the samples were examined by interpolating on a sigmoid four-parameter logistic regression standard curve.

Statistical Analysis

All experiments were performed in triplicate at a minimum. The data were expressed as mean ± standard deviations and analyzed by one-way analysis of variance (ANOVA) and the least-significant difference (LSD) test. Statistical significance was set at $p < 0.05$. The statistical analysis was performed with SPSS version 20.0 (SPSS, USA).

Results

Characterization of SPION@SS-31

The representative TEM images revealed that both SPION and SPION@SS-31 have good dispersibility and uniform spherical shape. A single crystal structure with single crystallinity and lattice stripes was observed in SPION or SPION@SS-31 (Fig. 2A). The surface charge (Zeta potential) of SPION@SS-31 synthesized in this experiment, exhibited a value of − 26.9 ± − 6.51 mV (Fig. 2B), which represents the stability of this particle. The hydrodynamic diameter distribution of SPION@SS-31 in PBS has a single peak and the Z-average particle size was 28.38 ± 0.32 nm (n = 3) (Fig. 2C). The hydrodynamic particle sizes of the SPION@SS-31 are generally larger than those detected by TEM due to the potential drop indicating the shrinkage of the hydration layer on the outside of the SPION@SS-31 in PBS and the reduction of charge-charge interactions after loading SS-31. The magnetization curve of SPION@SS-31 confirmed the good superparamagnetic character of SPION@SS-31 at room temperature since high magnetization and lack of hysteresis were observed. The magnetization trajectory was a single curve that passed through the origin. The saturation magnetization of the SPION@SS-31 is 54.26 emu/g (Fig. 2D), suggesting that loading SS-31 did not affect the superparamagnetic property of SPION. The time course

of SS-31 releasing from the SPION@SS-31 showed that SS-31 was rapidly released 70% within the first 12 hours, and then entered the slow release phase and lasted until 120 hours. (Fig. 2E).

[Figure 2 near here]

The Internalization of SPION@SS-31 and Macrophages Morphological Alteration

The internalization of SPION@SS-31 or SPION was determined using Prussian blue staining, SEM and TEM. After 24 hours of incubation, compared to the control group, Prussian blue staining clearly demonstrated the iron oxide nanoparticles were engulfed by macrophages. (Fig. 3A). SEM and TEM images confirmed the accumulation of SPION@SS-31 in macrophages (Fig. 3B, C). Forward Scatter (FSC) and Side Scatter (SSC) obviously increase in flow cytometry plots of macrophages from the SPION group than those of the control group (Fig. 3D). The FSC is related to the cell size, while the SSC is related to the cell granularity and complexity. The increased FSC implies enlarged cell size, whereas the increased SSC might indicate that cells became more irregular, evidenced by pseudopodia and protrusions on the surface of the cells (Fig. 3E). This phenomenon might imply the enhanced particles phagocytic activities, increased presence of vesicles in the cells like autophagy and increased cell apoptosis. Interestingly, macrophages in the SPION@SS-31 group appeared to have only a mild effect. In addition, the number of cell fragments increase in the SPION group than that of the SPION@SS-31 group (Fig. 3D), which suggested the SPION caused the cell damage but the adverse effect was relatively slight in the SPION@SS-31 group.

[Figure 3 near here]

SPION@SS-31 Mitigates Cell Apoptosis Induced by SPION

Cell viability in the SPION group was remarkably lower than that of the control and the SPION@SS-31 groups (both $p < 0.05$) (Fig. 4A). Compared with the SPION@SS-31 group, flow cytometry analysis showed the ratio of early apoptosis cells remarkably increased to almost 17% in the SPION group (both $p < 0.05$) (Fig. 4B, C). Notably, the ratio of early apoptosis cells in the SPION@SS-31 group were reduced to half of the SPION group (almost 8%). Even though cell viability and early apoptosis ratio were different between the SPION@SS-31 and the Control groups (both $p < 0.05$), these data still suggest that the macrophage toxicity caused by SPION could be significantly mitigated through SS-31 released from SPION@SS-31.

[Figure 4 near here]

SPION@SS-31 Improves Mitochondrial Damage Induced by SPION

To detect the level of oxidative stress, flow cytometry was performed to evaluate ROS production among the three groups. MFI of H2DCFDA images revealed that ROS production in the SPION group was almost

6 times more than those in the SPION@SS-31 group ($P < 0.05$) (Fig. 5A-B). After 24 hours SPION incubation, TEM images showed severe destruction of mitochondrial structure, including mitochondrial swelling, vacuolation, and mitochondrial crest rupture. However, similar mitochondrial damage in the SPION@SS-31 group was relatively mild. The damage score of mitochondrial structure from the SPION@SS-31 group was only half of the SPION group ($P < 0.05$) (Fig. 5C-D), suggesting that SPION@SS-31 could release SS-31 to significantly inhibit mitochondrial damage mediated by SPION. Mitochondrial ROS detection also exhibited that red fluorescence increased more significantly in the SPION group compared to the SPION@SS-31 group, in which remarkable red fluorescence dramatically decreased ($P < 0.05$, Fig. 5E-F). Interestingly, mitochondrial ROS production was comparable between the SPION@SS-31 and the control groups ($p > 0.05$, Fig. 5F). These results suggested that SPION significantly induced oxidative stress of macrophages, but this adverse effect could be rescued by SS-31 released from SPION@SS-31.

[Figure 5 near here]

SPION@SS-31 Inhibits Polarization of Macrophages to M1-Like Macrophages Induced by SPION

We further examined the phenotype and secretory function of macrophages after treatment with different nanoparticles. Compared with the control group, the SPION group demonstrated markedly up-regulated levels of IL-6 and TNF-α and expression of CD80 and CD86 ($P < 0.05$, Fig. 6A, B, E, F, I, J), suggesting that SPION have the potential to induce macrophages to polarize into pro-inflammatory M1-like subtype. Surprisingly, the levels of TNF-α secretion and the expression of CD80 and CD86 in the SPION@SS-31 group were significantly lower than those in the SPION group ($P < 0.05$, Fig. 6A, B, E, F, I). Moreover, the expression of CD163 was obviously up-regulated in the SPION@SS-31 group compared to the control and the SPION groups ($P < 0.05$, Fig. 6C, G), and the expression of CD80 and CD86 showed no significant change between the control group and the SPION@SS-31 group ($P > 0.05$, Fig. 6E-F). Correspondingly, the concentration of IL-10 and TGF-β in the SPION@SS-31 group was markedly higher than those in the SPION group ($P < 0.05$, Fig. 6K, L). There was no significant difference in the expression of CD206 among the three groups ($P > 0.05$, Fig. 6D, H). Taken together, these data indicated that SPION@SS-31 could not only significantly inhibit the polarization of macrophages to the M1-like subtype induced by SPION, but has the potential to promote the polarization of macrophages to anti-inflammatory M2-like subtype.

[Figure 6 near here]

Discussion

In the previous study, we observed that after intramyocardial transplantation of SPION labeled MSCs, SPION, as foreign bodies, induced a large number of macrophages infiltration in peripheral zones of myocardial infarction, which potentially aggravated the inflammatory response of infarcted myocardium, thereby provoking a concern whether SPION could trigger a pro-inflammatory effect when applied in cardiovascular field [26]. Macrophages at days 1–3 following myocardial infarction are dominated by

classically activating pro-inflammatory M1 subtype, which secrete cytokines, chemokines, growth factors, and matrix metalloproteinase to clear up the cell debris and degrade the extracellular matrix. M1 macrophages polarize into alternative anti-inflammatory M2 subtype at days 5–7 post-myocardial infarction. In contrast, M2 macrophages are preparative, which produce anti-inflammatory, preparative and proangiogenic factors (examples, IL-10, TGF-β1 and vascular endothelial growth factor) and remove dead cells to promote neovascularization and scar repair [27, 28]. However, the persistence of M1 macrophages can result in an expansion of infarct size and hinder the resolution of inflammation and scar formation [29].

Disturbingly, SPION have been reported to inhibit tumor growth by inducing macrophage polarization to pro-inflammatory subtype in tumor tissues [13]. Different morphology of SPION can induce pyroptosis, inflammasome activation and IL-1β secretion, especially the plate and octapod SPION demonstrating significantly higher activity than the sphere and cube SPION [30]. The above results implied the possibility that the SPION, when employed as therapeutic substance carriers or magnetic resonance contrast agents in ischemic myocardium, may disturb the shift of macrophages from M1 to M2 by inducing the prolonged pro-inflammatory effect, thereby impeding the repair process after myocardial infarction.

Moreover, it has been proved that compared to normo-ferremic ApoE-/- mice, atherosclerosis is dramatically aggravated in iron-loaded ApoE-/- $FPN^{wt/C326S}$ mice, indicating that iron can promote the progression of atherosclerosis. Excess iron deposits in the arterial media layer, facilitating vascular oxidative stress, dysfunction and plaque formation. Atherosclerosis is aggravated by iron-provoked vascular permeabilization, persistent endothelial activation, increased pro-atherogenic inflammatory mediators, lipid profile alterations, and reduced nitric oxide availability. Correspondingly, iron chelation therapy and a low-iron diet significantly alleviated the severity of the disease in ApoE-/-$FPN^{wt/C326S}$ mice [31]. Recently, SPION have been used as contrast agents to visualize atherosclerotic plaque, for they are easy to be internalized by macrophages in atherosclerotic plaque [32]. Another concern is that SPION might induce iron overload at the cellular level after being internalized and degraded by macrophages in the plaque, aggravating plaque progression or promoting plaque instability through mediating oxidative stress, pro-inflammatory effect and endothelial cell dysfunction. Good safety and biocompatibility are the necessary prerequisites for the clinical transformation of SPION. Therefore, it is urgent to explore strategies to improve the biosafety of SPION.

SPION have been confirmed to damage a variety of organelles by inducing ROS generation, including Golgi stress, destruction of lysosome and mitochondria and over activated endoplasmic reticulum stress and autophagy [17, 33], especially mitochondria, as the energy factory of cells, is very crucial to maintain energy metabolism and physiological function. Furthermore, mitochondria are also the largest iron metabolism organelle and the main place for ROS production in cells. Thus, mitochondria are speculated to be the main target organelle of SPION [11, 34].

Mitochondrial targeted antioxidant peptides have been confirmed to play a strong protective role against ischemic brain injury and kidney ischemia-reperfusion injury [35, 36]. In particular, SS-31 (D-Arg-DMT-Lys-

Phe-NH2) has been proved to be the most effective protective agent against ischemia-reperfusion injury in SS peptides [37, 38]. After entering mitochondria, tyrosine residues on SS-31 polypeptide scavenge ROS by forming inactive tyrosyl groups, significantly inhibit ROS production and reduce lipid peroxidation and cardiomyocyte death, eventually reducing infarct size [39, 40]. In view of this, SS-31 might bear the potential to improve the cardiovascular safety of SPION by protecting mitochondria.

We first prepared negatively charged SPION as previously described [17], and then successfully constructed SPION@SS-31 by PEI mediated adsorption (Fig. 1). Our data showed that compared with the control group, SPION induced loss of viability and increase of early apoptosis, up-regulated the expression of CD86 and CD80 (M1-like subtype markers) and down-regulated the expression of CD163 (M2-like subtype marker) in macrophages, accompanied by the increased secretion of TNF-α and IL-6 and the decreased secretion of TGF-β and IL-10, strongly suggesting that SPION can induce the polarization of macrophages into pro-inflammatory M1-like subtype in vitro study. Interestingly, compared with the control group, SPION@SS-31 only induced a slight loss of cell viability and early apoptosis of macrophages after 24 hours of treatment. Notably, SPION@SS-31-treated cells demonstrated that the expression of CD163 was up-regulated and the expression of CD86 and CD80 was down-regulated, along with the decreased secretion of TNF-α and increased secretion of TGF-β and IL-10. Meanwhile, we observed that the SPION induced a significant increase in the level of ROS and serious damage to the mitochondria, characterized by mitochondrial swelling, blurring of mitochondrial cristae and vacuolation, implying that oxidative stress and mitochondrial damage might be the main toxic mechanism of SPION. The level of cellular ROS and the mitochondrial damage in the SPION@SS-31 group were significantly lower than those in the SPION group. All these suggested that after internalized by macrophages, SPION@SS-31 can release the active form of SS-31 to the mitochondrial inner membrane, where it exerts a mitochondrial targeted antioxidant effect, protecting mitochondria from oxidative stress damage mediated by Fenton reaction catalyzed by SPION degradation to ferrous ion. Moreover, SPION@SS-31 exhibited a tendency to induce macrophages to polarize to M2-like subtype even though there is no significant difference in the expression of CD206 between the SPION and the SPION@SS-31 groups. At the present study we only detected mitochondrial structure and oxidative stress injury. Further detection of the downstream molecular mechanism of oxidative stress, including proteins related to iron metabolism, such as ferritin, iron exporter ferroprotein, transferrin, and signaling pathways of pyroptosis [30, 41] or ferroptosis [42, 43], which have been reported in other studies would be investigated in future work.

Previous studies have confirmed that the cytotoxicity of SPION is time and concentration dependent [44–46]. Here, we only detected the cellular events of a moderate concentration of 50μg/ml Fe_3O_4 at 24-hour observation. The time course of SS-31 releasing from the SPION@SS-31 exhibited that SS-31 has the potential to maintain the effective concentration for at least 96 hours, thereby it is possible to stably play the mitochondrial targeted antioxidant effect in higher concentration and longer observation.

Our previous study has confirmed that the M-MSN@NAC can attenuate cytotoxicity of iron oxide nanoparticles in hypoxia/reoxygenation cardiomyocytes. However, our in vivo experiments showed that

M-MSN@NAC only mildly improved the negative left ventricular remodeling mediated by iron oxide nanoparticles in a rat model of myocardial ischemia-reperfusion (data not published). We speculated that the unsatisfactory result was attributed to the fact that NAC was rapidly released 72% within 2.5 hours, and only lasted until 48 hours [17], so it is difficult to play a long-term protective role in animal experiments; More importantly, we observed that the main target organelle of iron oxide nanoparticles is mitochondria, whereas NAC has no mitochondrial targeting function, so it failed to prevent mitochondria against ROS attack. Thus, we determined to employ mitochondrial targeted antioxidant SS-31 to modify SPION. The observation of 24 hours in vitro has been shown SPION@SS-31 can effectively inhibit the pro-inflammatory effect induced by SPION. Next, we will plan to construct a sustained release system of SPION@SS-31 by polyethylene glycol (PEG) modification, maintaining the long-term effective concentration of SS-31 in vivo study, in which PEG has been employed in preparing drug sustained-release delivery system with good biocompatibility [47, 48].

Our study demonstrated for the first time that the modification of mitochondrial targeted antioxidant SS-31 can significantly inhibit the pro-inflammatory effect mediated by SPION. Considering that the pro-inflammatory effect mediated by SPION may impede the repair of infarcted heart or induce plaque instability, it is particularly important to improve the cardiovascular safety of SPION. The SS-31 modification is expected to be a promising strategy to improve the cardiovascular safety of SPION, which needs to be further verified by animal experiments.

Conclusion

SPION can promote macrophages polarization to the M1-like subtype by inducing oxidative stress and mitochondrial damage, while SPION@SS-31 could significantly inhibit macrophage toxicity mediated by SPION via releasing SS-31 and has the potential to induce macrophages polarization to M2-like subtype.

Abbreviations

SPION
Superparamagnetic iron oxide nanoparticles
ROS
reactive oxygen species
ELISA
enzyme-linked immunosorbent assay
TEM
transmission electron microscope
DLS
Dynamic light scattering
SEM
scanning electron microscope
FSC

forward scatter
SSC
side scatter
CCK-8
Cell Counting Kit-8
MFI
median fluorescence intensity
ANOVA
one-way analysis of variance
OD
optical density
NAC
N-acetylcysteine
PEG
polyethylene glycol

Declarations

Ethics approval and consent to participate

Not applicable.

Consent for publication

All authors provided consent for publication.

Availability of Data and Materials

The original contributions presented in the study are included in the article, further inquiries can be directed to the corresponding author.

Competing interests

The author reports no conflicts of interest in this work.

Funding

This work was funded by Natural Science Foundation of Jiangxi Province of China (20192BAB205006); Top-level Clinical Discipline Project of Shanghai Pudong District (PWYgf2021-01); Training plan for discipline leaders of Shanghai Pudong New Area Health Commission (PWRd2020-09); the Health Science and Technology Project of Shanghai Pudong New Area Health Commission (PW2019A-13).

Authors' contributions

Qizheng Lu and Haibo Liu contributed equally to this work.

Yunli Shen and Ning Pei finished study design, Qizheng Lu and Haibo Liu finished experimental studies, Hao Zheng, Youming Zhang, Jinbo Ou, Jieyun You, Jingjiang Pi and Xiaobo Yao finished data analysis. Qi Zhang, Jing Xu, Xingxu Wang, Yunkai Wang assisted with the optimization and proofed the manuscript. Qizheng Lu and Yunli Shen finished manuscript editing. All authors read and approved the final manuscript.

Acknowledgments

We would like to give our sincere gratitude to the reviewers for their constructive comments.

References

1. Avasthi A, Caro C, Pozo-Torres E, Leal MP, García-Martín ML. (2020)Magnetic Nanoparticles as MRI Contrast Agents. Top Curr Chem (Cham).378(3):40.
2. Mathiasen AB, Qayyum AA, Jørgensen E, Helqvist S, Ekblond A, Ng M, et al. (2019)In Vivo MRI Tracking of Mesenchymal Stromal Cells Labeled with Ultrasmall Paramagnetic Iron Oxide Particles after Intramyocardial Transplantation in Patients with Chronic Ischemic Heart Disease. Stem Cells Int.2019:2754927.
3. Huang Z, Shen Y, Pei N, Sun A, Xu J, Song Y, et al. (2013)The effect of nonuniform magnetic targeting of intracoronary-delivering mesenchymal stem cells on coronary embolisation. Biomaterials.34(38):9905–9916.
4. Yang H, Wei L, Liu C, Zhong W, Li B, Chen Y, et al. (2019)Engineering human ventricular heart tissue based on macroporous iron oxide scaffolds. Acta Biomater.88:540–553.
5. Anselmo AC, Mitragotri S. (2019)Nanoparticles in the clinic: An update. Bioeng Transl Med.4(3):e10143-e10143.
6. Alam SR, Stirrat C, Richards J, Mirsadraee S, Semple SI, Tse G, et al. (2015)Vascular and plaque imaging with ultrasmall superparamagnetic particles of iron oxide. J Cardiovasc Magn Reson.17(1):83.
7. Stirrat CG, Alam S, MacGillivray TJ, Gray C, Dweck MR, Jones V, et al. (2019)Ferumoxytol-enhanced MRI in patients with prior cardiac transplantation. Open Heart.6(2):e001115.
8. Yilmaz A. (2017)Visualising inflammation after myocardial infarction with the use of iron oxide nanoparticles. Heart.103(19):1479–1480.
9. Stirrat CG, Alam SR, MacGillivray TJ, Gray CD, Dweck MR, Dibb K, et al. (2018)Ferumoxytol-enhanced magnetic resonance imaging in acute myocarditis. Heart.104(4):300–305.
10. Scally C, Abbas H, Ahearn T, Srinivasan J, Mezincescu A, Rudd A, et al. (2019)Myocardial and Systemic Inflammation in Acute Stress-Induced (Takotsubo) Cardiomyopathy. Circulation.139(13):1581–1592.

11. Zheng H, You J, Yao X, Lu Q, Guo W, Shen Y. (2020)Superparamagnetic iron oxide nanoparticles promote ferroptosis of ischemic cardiomyocytes. Journal of cellular and molecular medicine.24(18):11030–11033.
12. Laskar A, Eilertsen J, Li W, Yuan XM. (2013)SPION primes THP1 derived M2 macrophages towards M1-like macrophages. Biochem Biophys Res Commun.441(4):737–742.
13. Zanganeh S, Hutter G, Spitler R, Lenkov O, Mahmoudi M, Shaw A, et al. (2016)Iron oxide nanoparticles inhibit tumour growth by inducing pro-inflammatory macrophage polarization in tumour tissues. Nat Nanotechnol.11(11):986–994.
14. ter Horst EN, Hakimzadeh N, van der Laan AM, Krijnen PA, Niessen HW, Piek JJ. (2015)Modulators of Macrophage Polarization Influence Healing of the Infarcted Myocardium. Int J Mol Sci.16(12):29583–29591.
15. Yang S, Yuan HQ, Hao YM, Ren Z, Qu SL, Liu LS, et al. (2020)Macrophage polarization in atherosclerosis. Clin Chim Acta.501:142–146.
16. Stroh A, Zimmer C, Gutzeit C, Jakstadt M, Marschinke F, Jung T, et al. (2004)Iron oxide particles for molecular magnetic resonance imaging cause transient oxidative stress in rat macrophages. Free Radic Biol Med.36(8):976–984.
17. Shen Y, Gong S, Li J, Wang Y, Zhang X, Zheng H, et al. (2019)Co-loading antioxidant N-acetylcysteine attenuates cytotoxicity of iron oxide nanoparticles in hypoxia/reoxygenation cardiomyocytes. International journal of nanomedicine.14:6103–6115.
18. Battaglia AM, Chirillo R, Aversa I, Sacco A, Costanzo F, Biamonte F. (2020)Ferroptosis and Cancer: Mitochondria Meet the "Iron Maiden" Cell Death. Cells.9(6).
19. Lee FY, Shao PL, Wallace CG, Chua S, Sung PH, Ko SF, et al. (2018)Combined Therapy with SS31 and Mitochondria Mitigates Myocardial Ischemia-Reperfusion Injury in Rats. Int J Mol Sci.19(9).
20. Shang L, Ren H, Wang S, Liu H, Hu A, Gou P, et al. (2021)SS-31 Protects Liver from Ischemia-Reperfusion Injury via Modulating Macrophage Polarization. Oxid Med Cell Longev.2021:6662156.
21. Gibson CM, Giugliano RP, Kloner RA, Bode C, Tendera M, Jánosi A, et al. (2016)EMBRACE STEMI study: a Phase 2a trial to evaluate the safety, tolerability, and efficacy of intravenous MTP-131 on reperfusion injury in patients undergoing primary percutaneous coronary intervention. Eur Heart J.37(16):1296–1303.
22. Zhao K, Zhao GM, Wu D, Soong Y, Birk AV, Schiller PW, et al. (2004)Cell-permeable peptide antioxidants targeted to inner mitochondrial membrane inhibit mitochondrial swelling, oxidative cell death, and reperfusion injury. J Biol Chem.279(33):34682–34690.
23. Wang Q, Shen M, Zhao T, Xu Y, Lin J, Duan Y, et al. (2015)Low toxicity and long circulation time of polyampholyte-coated magnetic nanoparticles for blood pool contrast agents. Sci Rep.5:7774.
24. Miao C, Hu F, Rui Y, Duan Y, Gu H. (2019)A T(1)/T(2) dual functional iron oxide MRI contrast agent with super stability and low hypersensitivity benefited by ultrahigh carboxyl group density. J Mater Chem B.7(12):2081–2091.

25. Flameng W, Borgers M, Daenen W, Stalpaert G. (1980)Ultrastructural and cytochemical correlates of myocardial protection by cardiac hypothermia in man. J Thorac Cardiovasc Surg.79(3):413–424.
26. Huang Z, Li C, Yang S, Xu J, Shen Y, Xie X, et al. (2015)Magnetic resonance hypointensive signal primarily originates from extracellular iron particles in the long-term tracking of mesenchymal stem cells transplanted in the infarcted myocardium. International journal of nanomedicine.10:1679–1690.
27. Gombozhapova A, Rogovskaya Y, Shurupov V, Rebenkova M, Kzhyshkowska J, Popov SV, et al. (2017)Macrophage activation and polarization in post-infarction cardiac remodeling. J Biomed Sci.24(1):13.
28. Ma Y, Mouton AJ, Lindsey ML. (2018)Cardiac macrophage biology in the steady-state heart, the aging heart, and following myocardial infarction. Transl Res.191:15–28.
29. Leuschner F, Dutta P, Gorbatov R, Novobrantseva TI, Donahoe JS, Courties G, et al. (2011)Therapeutic siRNA silencing in inflammatory monocytes in mice. Nat Biotechnol.29(11):1005–1010.
30. Liu L, Sha R, Yang L, Zhao X, Zhu Y, Gao J, et al. (2018)Impact of Morphology on Iron Oxide Nanoparticles-Induced Inflammasome Activation in Macrophages. ACS Appl Mater Interfaces.10(48):41197–41206.
31. Vinchi F, Porto G, Simmelbauer A, Altamura S, Passos ST, Garbowski M, et al. (2020)Atherosclerosis is aggravated by iron overload and ameliorated by dietary and pharmacological iron restriction. Eur Heart J.41(28):2681–2695.
32. Montiel Schneider MG, Lassalle VL. (2017)Magnetic iron oxide nanoparticles as novel and efficient tools for atherosclerosis diagnosis. Biomed Pharmacother.93:1098–1115.
33. Zhang X, Zhang H, Liang X, Zhang J, Tao W, Zhu X, et al. (2016)Iron Oxide Nanoparticles Induce Autophagosome Accumulation through Multiple Mechanisms: Lysosome Impairment, Mitochondrial Damage, and ER Stress. Mol Pharm.13(7):2578–2587.
34. Peng Q, Huo D, Li H, Zhang B, Li Y, Liang A, et al. (2018)ROS-independent toxicity of Fe(3)O(4) nanoparticles to yeast cells: Involvement of mitochondrial dysfunction. Chem Biol Interact.287:20–26.
35. Birk AV, Liu S, Soong Y, Mills W, Singh P, Warren JD, et al. (2013)The mitochondrial-targeted compound SS-31 re-energizes ischemic mitochondria by interacting with cardiolipin. J Am Soc Nephrol.24(8):1250–1261.
36. Imai T, Mishiro K, Takagi T, Isono A, Nagasawa H, Tsuruma K, et al. (2017)Protective Effect of Bendavia (SS-31) Against Oxygen/Glucose-Deprivation Stress-Induced Mitochondrial Damage in Human Brain Microvascular Endothelial Cells. Curr Neurovasc Res.14(1):53–59.
37. Saad A, Herrmann SMS, Eirin A, Ferguson CM, Glockner JF, Bjarnason H, et al. (2017)Phase 2a Clinical Trial of Mitochondrial Protection (Elamipretide) During Stent Revascularization in Patients With Atherosclerotic Renal Artery Stenosis. Circ Cardiovasc Interv.10(9).
38. Cai J, Jiang Y, Zhang M, Zhao H, Li H, Li K, et al. (2018)Protective effects of mitochondrion-targeted peptide SS-31 against hind limb ischemia-reperfusion injury. J Physiol Biochem.74(2):335–343.

39. Shi J, Dai W, Hale SL, Brown DA, Wang M, Han X, et al. (2015)Bendavia restores mitochondrial energy metabolism gene expression and suppresses cardiac fibrosis in the border zone of the infarcted heart. Life Sci.141:170–178.
40. Dai W, Shi J, Gupta RC, Sabbah HN, Hale SL, Kloner RA. (2014)Bendavia, a mitochondria-targeting peptide, improves postinfarction cardiac function, prevents adverse left ventricular remodeling, and restores mitochondria-related gene expression in rats. J Cardiovasc Pharmacol.64(6):543–553.
41. Clerc P, Jeanjean P, Hallali N, Gougeon M, Pipy B, Carrey J, et al. (2018)Targeted Magnetic Intra-Lysosomal Hyperthermia produces lysosomal reactive oxygen species and causes Caspase-1 dependent cell death. Journal of controlled release: official journal of the Controlled Release Society.270:120–134.
42. Sang M, Luo R, Bai Y, Dou J, Zhang Z, Liu F, et al. (2019)Mitochondrial membrane anchored photosensitive nano-device for lipid hydroperoxides burst and inducing ferroptosis to surmount therapy-resistant cancer. Theranostics.9(21):6209–6223.
43. Shen Z, Liu T, Li Y, Lau J, Yang Z, Fan W, et al. (2018)Fenton-Reaction-Acceleratable Magnetic Nanoparticles for Ferroptosis Therapy of Orthotopic Brain Tumors. ACS Nano.12(11):11355–11365.
44. Naqvi S, Samim M, Abdin M, Ahmed FJ, Maitra A, Prashant C, et al. (2010)Concentration-dependent toxicity of iron oxide nanoparticles mediated by increased oxidative stress. International journal of nanomedicine.5:983–989.
45. Khan MI, Mohammad A, Patil G, Naqvi SA, Chauhan LK, Ahmad I. (2012)Induction of ROS, mitochondrial damage and autophagy in lung epithelial cancer cells by iron oxide nanoparticles. Biomaterials.33(5):1477–1488.
46. Luo C, Li Y, Yang L, Wang X, Long J, Liu J. (2015)Superparamagnetic iron oxide nanoparticles exacerbate the risks of reactive oxygen species-mediated external stresses. Arch Toxicol.89(3):357–369.
47. Dorniani D, Kura AU, Hussein-Al-Ali SH, Bin Hussein MZ, Fakurazi S, Shaari AH, et al. (2014)In vitro sustained release study of gallic acid coated with magnetite-PEG and magnetite-PVA for drug delivery system. ScientificWorldJournal.2014:416354.
48. Zhang Y, Ding N, Zhang T, Sun Q, Han B, Yu T. (2019)A Tetra-PEG Hydrogel Based Aspirin Sustained Release System Exerts Beneficial Effects on Periodontal Ligament Stem Cells Mediated Bone Regeneration. Front Chem.7:682.

Figures

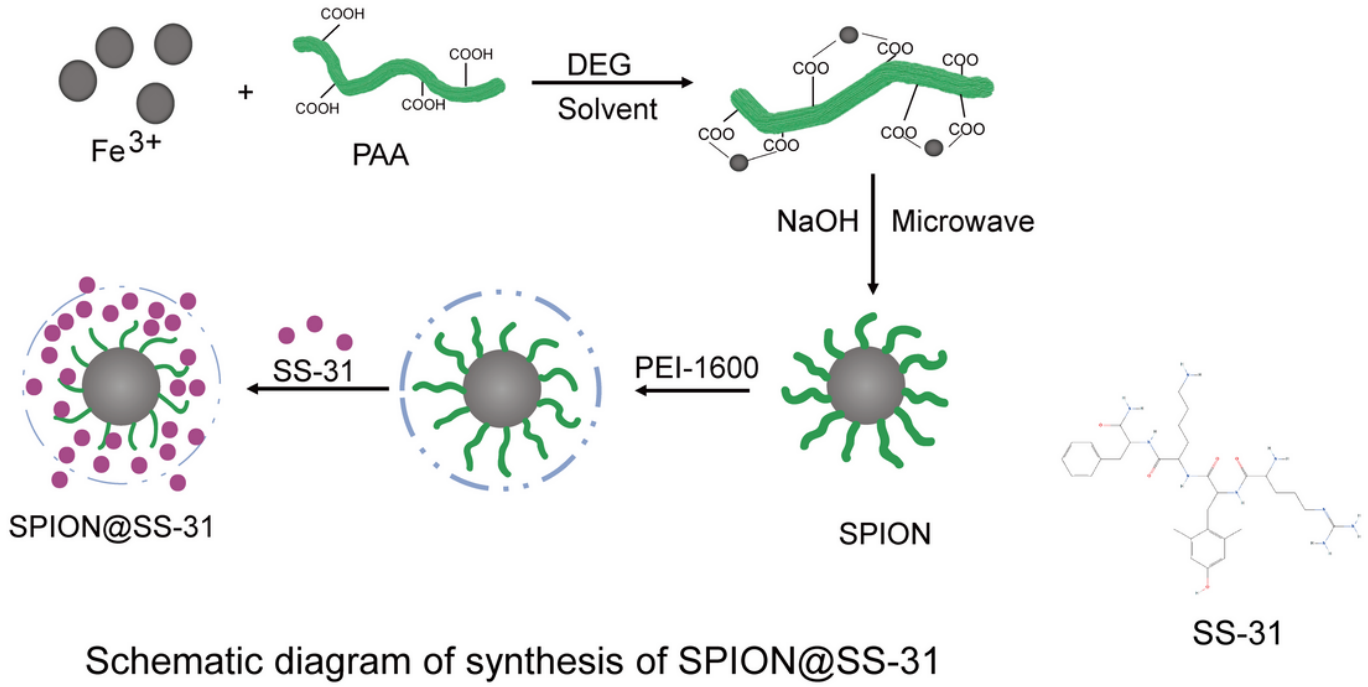

Figure 1

Schematic diagram of SPION@SS-31 synthesis

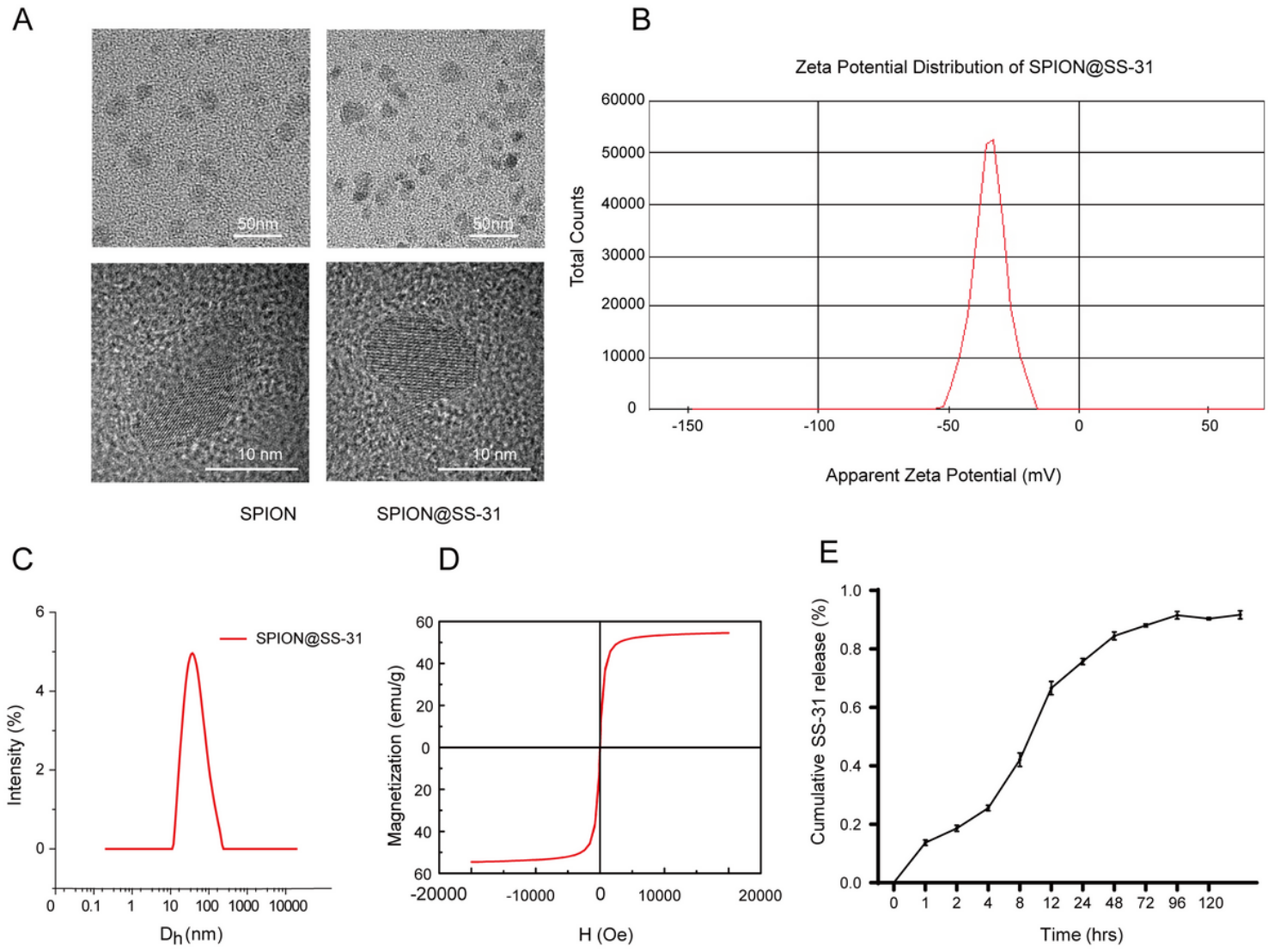

Figure 2

Characterization of SPION@SS-31. (A) Representative TEM images of SPION and SPION@SS-31. (B) Zeta potential distribution of SPION@SS-31. (C) Hydrodynamic diameter distribution of SPION@SS-31 in PBS. (D) Magnetization curve of SPION@SS-31. (E) Profile of SS-31 release from the SPION@SS-31 dissolved in PBS (pH=7.4) at 37°C. Data were collected from three independent experiments.

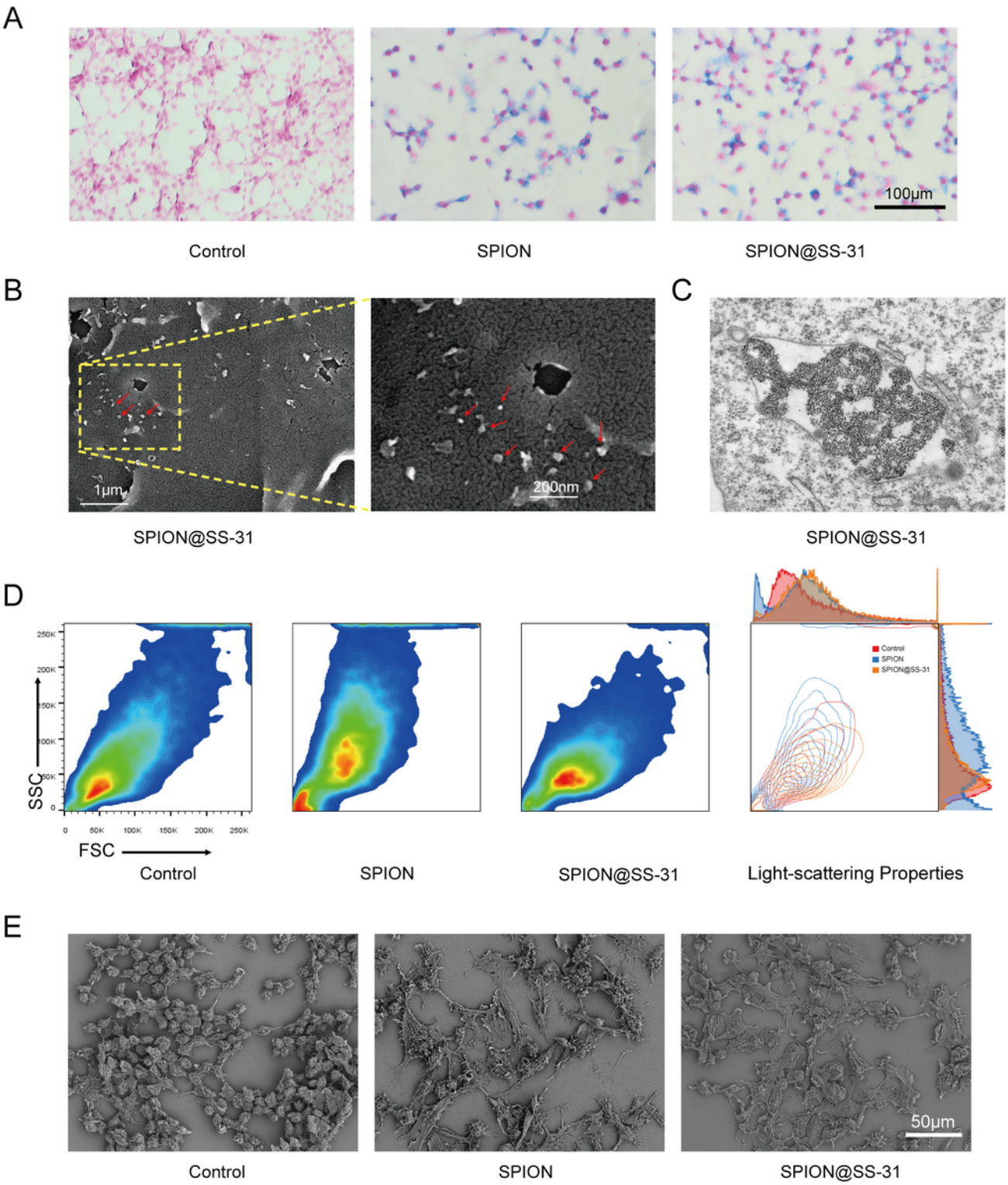

Figure 3

The internalization of SPION@SS-31 and macrophages morphological alteration. (A) Prussian blue staining images showed the accumulation of iron-containing nanoparticles in macrophages following incubation with SPION or SPION@SS-31 for 24h. (B) SEM image of the phagocytosis of SPION@SS-31, red arrows denote the SPION@SS-31. (C) TEM image of the macrophage phagocytosis of SPION@SS-31 (D) Representative flow cytometry pictures of FSC/SSC parameters showing the size and granularity of

macrophages following incubation with culture medium, SPION or SPION@SS-31 for 24h, respectively. (E) SEM image of macrophages following incubation with culture medium, SPION or SPION@SS-31 for 24h, respectively.

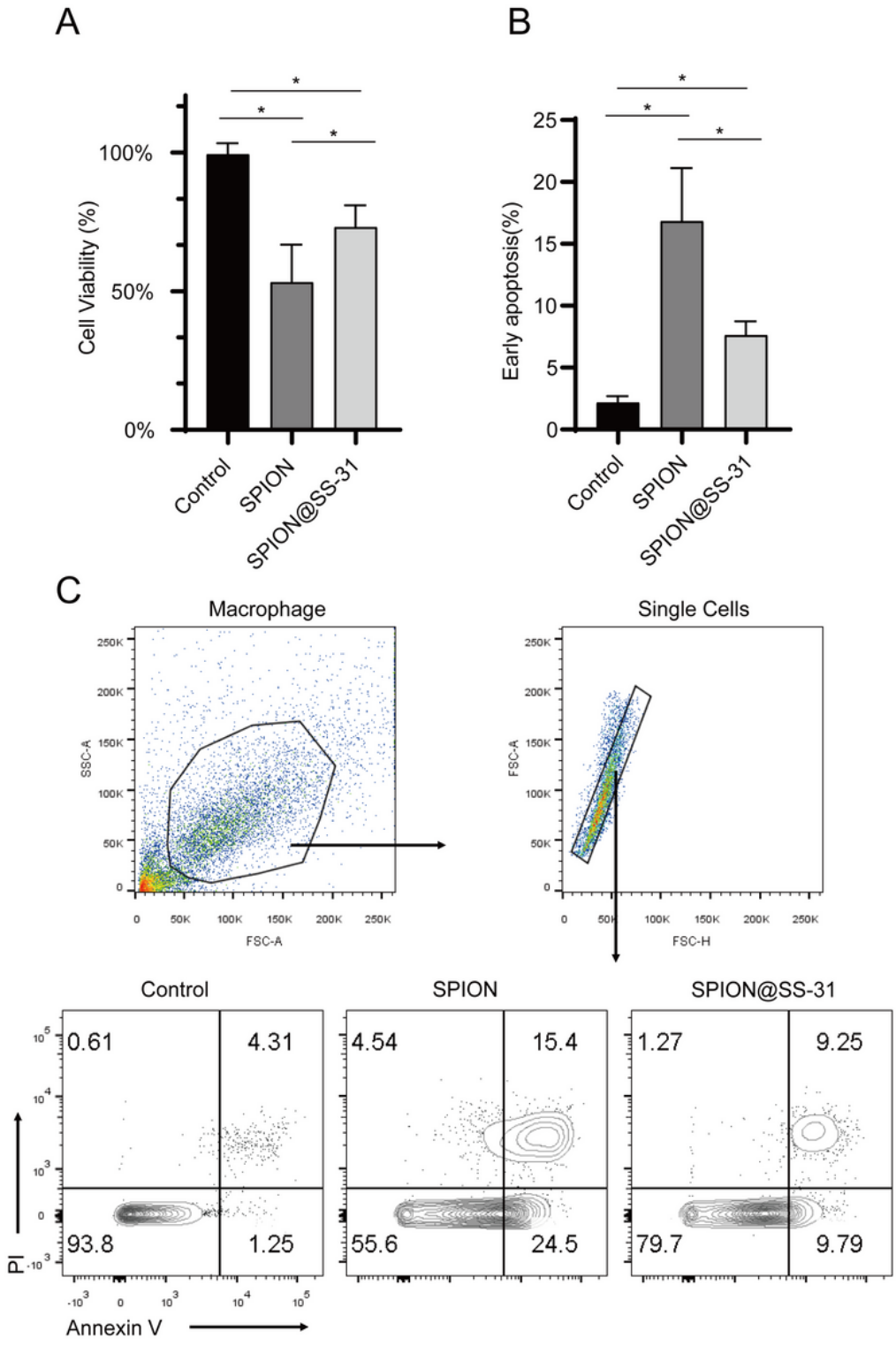

Figure 4

SPION@SS-31 mitigates cell apoptosis induced by SPION. (A) Macrophage viability after 24h incubation measured by CCK-8. (B) Flow cytometric early apoptosis scale of macrophages exposed to the culture medium, SPION or SPION@SS-31 for 24h, respectively. (C) Representative pictures of the apoptosis analysis of different groups. (*p<0.05)

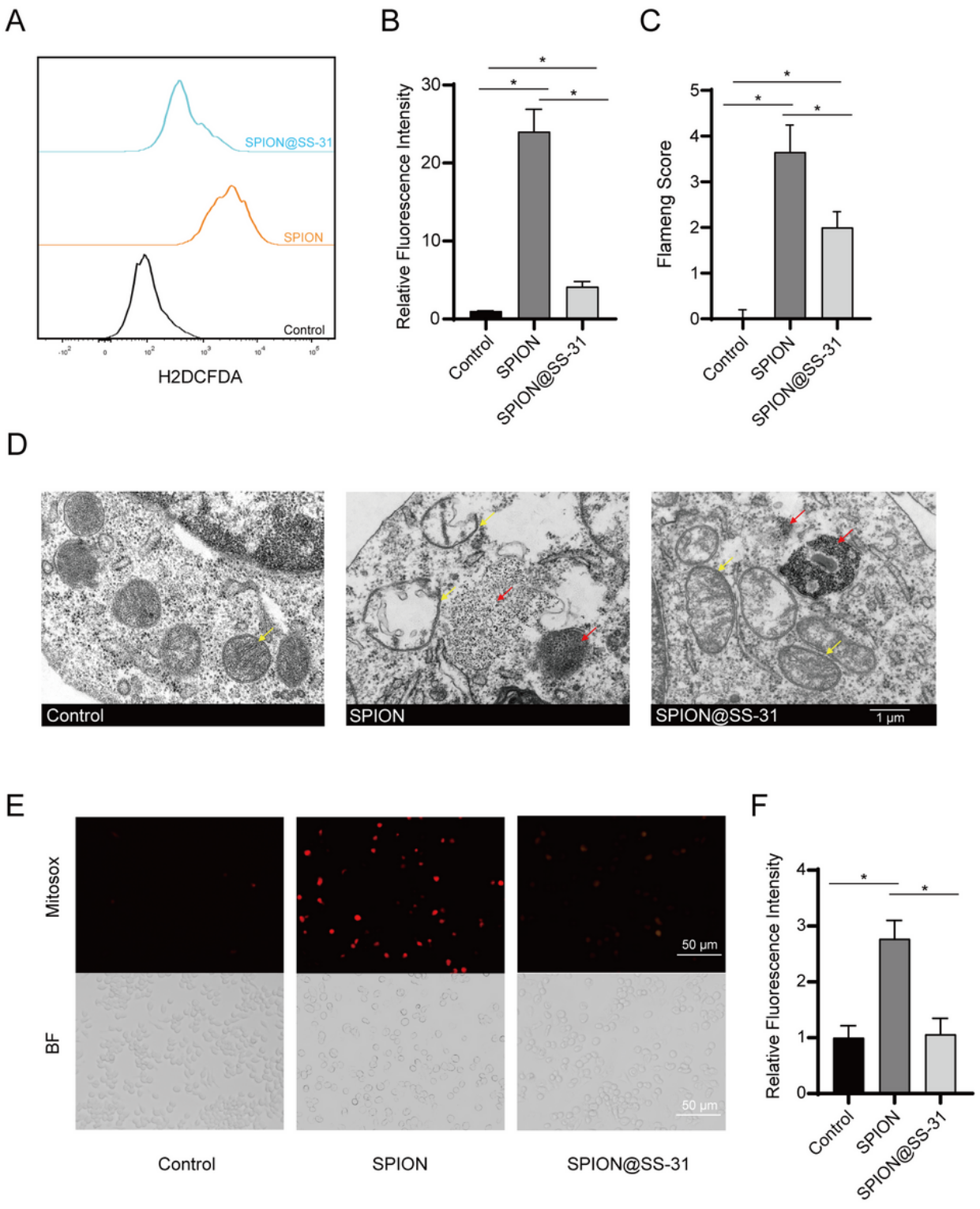

Figure 5

SPION@SS-31 improves mitochondrial damage induced by SPION. (A) ROS levels were measured by H2DCF-DA staining using flow cytometry. Lines from bottom to the top are black: control; orange: SPION and blue: SPION@SS-31, respectively. (B) Relative mean fluorescence intensity of different groups after H2DCF-DA staining. (C) Flameng score of mitochondrial damage assessment. (D) Representative TEM image of ultrastructure and organelles of macrophages exposed to different nanoparticles for 24h. Red arrows indicated the internalized nanoparticles; Yellow arrows indicated the mitochondria (E) Representative photomicrographs of mitochondrial ROS in macrophages treated with different nanoparticles. Red fluorescent intensity indicated ROS production. (F) Quantitative analysis of red fluorescent intensity in individual group. (*$p<0.05$).

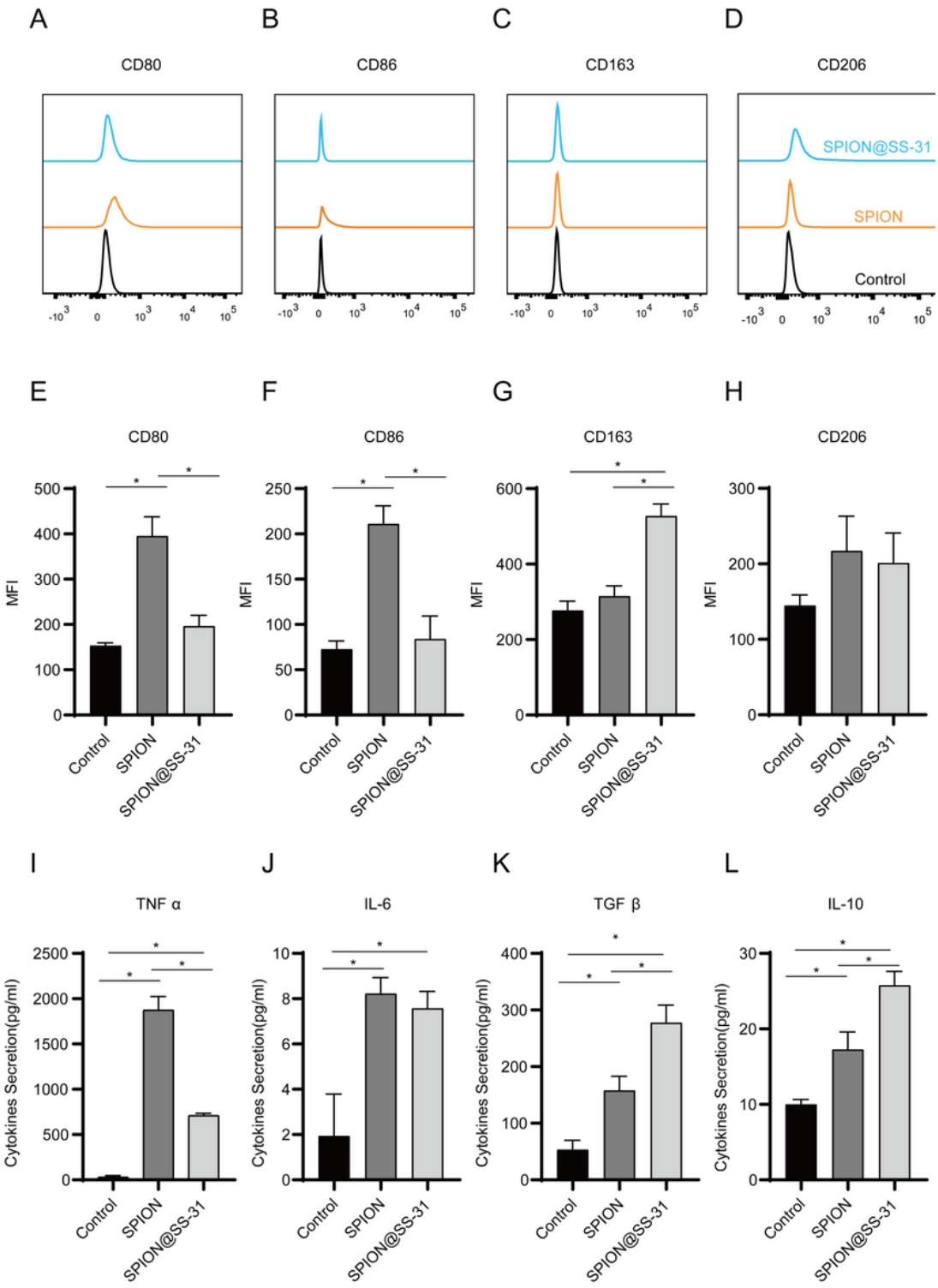

Figure 6

SPION@SS-31 inhibits polarization of macrophages to M1-Like macrophages induced by SPION. (A-D) Cell surface markers CD80, CD86, CD163, and CD206 expression were detected by flow cytometry. Lines from bottom to the top are black: control; orange: SPION; and blue: SPION@SS-31, respectively. (E-H) MFI of cell surface markers described above. (I-L) TNF-α, IL-6, TGF-β, and IL-10 production in the cell culture supernatant were detected by ELISA. (*p<0.05)